CVGIP: GRAPHICAL MODELS AND IMAGE PROCESSING
Vol. 53, No. 4, July, pp. 392–401, 1991

NOTE

Spline Models for Boundary Detection/Description: Formulation and Performance Evaluation

D. BRZAKOVIC

Department of Electrical and Computer Engineering, University of Tennessee, Knoxville, Tennessee 37996

AND

A. LIAKOPOULOS

Department of Mechanical Engineering and Mechanics, Lehigh University, Bethlehem, Pennsylvania 18015

AND

L. HONG

Department of Electrical Engineering, Wright State University, Dayton, Ohio 45435

Received January 31, 1989; accepted September 26, 1990

This paper describes a hybrid boundary detection method that locates smooth boundaries in noisy images. The boundary estimation involves two steps. The first step identifies statistically homogeneous regions and intermediate regions wherein boundaries lie. In the second step, boundaries are estimated using a linear recursive filter and statistical properties of the homogeneous regions. The boundaries are modeled by spline functions and the model is utilized in two different ways providing either an analytical description of the boundary or individual boundary points. The method has been applied to a number of images and the results are very good. © 1991 Academic Press, Inc.

1. INTRODUCTION

Determination of boundaries delimiting objects or parts of objects is recognized to be a crucial link between an image and its meaningful interpretation. Consequently, boundary detection has been the subject of extensive research endeavors. In this paper we propose a hybrid boundary detection method whose objective is to locate boundaries in noisy images based on statistical properties of adjacent regions. The problem of boundary detection is posed in the framework of estimation theory by: (1) formulating mathematical system models based on the assumed geometric boundary models, (2) utilizing statistical properties of the adjacent regions to develop linear measurement models, and (3) invoking a linear recursive filter (LRF) for boundary estimation. The spline-based boundary models, proposed in this paper, allow modeling of boundaries of arbitrary shapes, in contrast to other approaches, e.g., Refs. [1, 2]. Spline-based models were used in [10]; however, the objective of our approach is to detect boundaries between low contrast noisy regions or texture, that the energy minimization approach [10] may not detect. In addition, to achieve fast processing we use LRF, thus making the method well suited for real time applications. More importantly, LRF provides, through the error covariance matrix, a direct measure of the uncertainty in the estimated boundary.

The theoretical basis, implementation, and performance evaluation of the proposed boundary detection/description method is presented in this paper. Section 2 discusses the formulation of the problem of boundary estimation in the framework of linear recursive filtering. Section 3 details two approaches of utilizing the boundary model, while application issues and results are presented in Section 4.

2. PROBLEM FORMULATION

The boundary estimation method described in this paper involves two steps. The first step identifies statistically homogeneous regions, A and B, and the intermediate region, W, hereafter called *ambiguity zone* (Fig. 1). This step reduces the problem of estimating a boundary between regions of unknown properties to the problem of boundary estimation between regions of known properties. An approach to determining the ambiguity zone is detailed in [3] and an example of an ambiguity zone is

1049-9652/91 $3.00

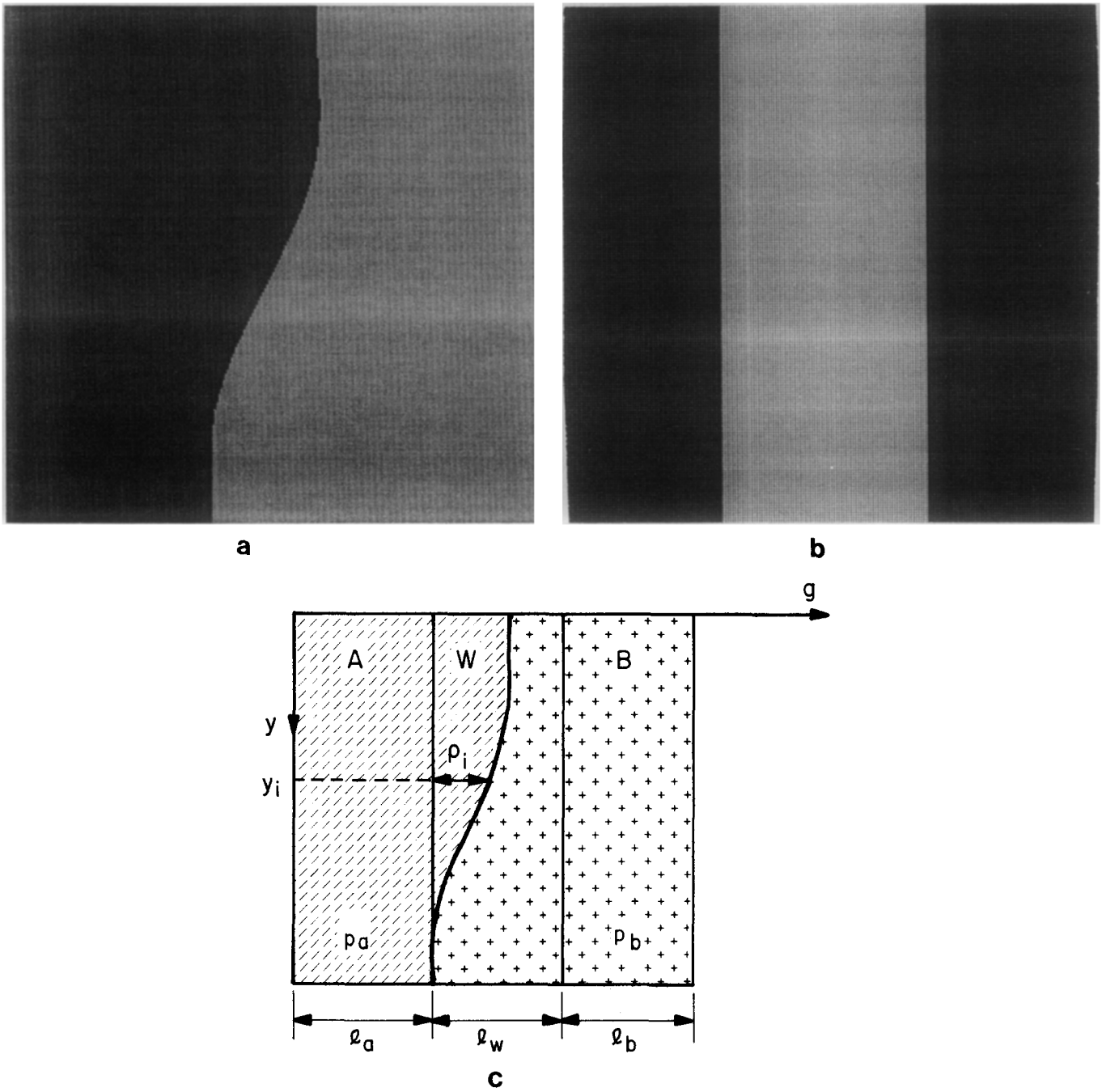

FIG. 1. Ambiguity zone between statistically homogeneous regions: (a) original image, (b) rectangular ambiguity zone, (c) notation.

shown in Fig. 1. The second step is the actual boundary estimation. The two-step processing is recognized to be a viable approach to difficult segmentation problems and has been used in problems of texture segmentation, e.g., Ref. [6].

The objective of the boundary estimator is to determine the boundary location based on noisy measurements performed in the ambiguity zone. In this work, spline functions are used to approximate each boundary. By approximating a boundary in W by a spline function, we formulate system and measurement models of the form

$$\begin{aligned} \boldsymbol{x}_{k+1} &= \Phi_k \boldsymbol{x}_k + \boldsymbol{w}_k, \quad \boldsymbol{w}_k \sim N(0, Q_k) \\ \boldsymbol{z}_k &= H_k \boldsymbol{x}_k + \boldsymbol{v}_k \quad \boldsymbol{v}_k \sim N(0, R_k), \end{aligned} \tag{1}$$

where $\boldsymbol{x}_k$ denotes the state vector, $\boldsymbol{z}_k$ contains the noisy measurements, and $\boldsymbol{w}_k$ and $\boldsymbol{v}_k$ are system and measure-

ment noise vectors, respectively. Different boundary approximation models result in different system matrices, Φ_k, and measurement matrices, H_k. With Eqs. (1) at our disposal, LRF [9] is employed to estimate the state vector x_k as described in [5].

3. FORMULATION OF MEASUREMENT AND SYSTEM MODELS

In the following for simplicity, we present the measurement and system models for vertical boundaries. Boundary of any orientation can be treated using this formulation (except for a horizontal boundary, in which case it is necessary to incorporate rotation of the coordinate system by 90°). The measurement model relates the values of a property p in the statistically homogeneous regions A and B to the value of property p in the ambiguity zone, W, at $y = \text{const}$. The selection of an appropriate property p for specific families of images is discussed in Section 4. In essence, the measurement model replaces measurements of a particular boundary point coordinate (ρ_i in Fig. 1) by measurements of a chosen property in regions A, B, W, or their parts. The formulation presented in this section is independent of the choice of property p as long as the assumption of linear dependence on the states [Eq. (1)] is satisfied. Assuming that p_i, i.e., the value of property p in W at $y = \bar{y}_i = \text{const}$, is a linear combination of p_a and p_b, their relationship (see Fig. 1) is

$$p_i = \frac{p_a\rho_i + (l_w - \rho_i)p_b}{l_w}. \tag{2}$$

Multiple measurements are performed simultaneously in different regions of the ambiguity zone to ensure observability of all states. In general, we consider m simultaneous measurements performed along windows of dimensions $s \times l$ centered in the y-direction at $\bar{y}_j$, $j = 1, 2, \ldots, m$. In Sections 3.1 and 3.2, we formulate two system and measurement models of the form of Eq. (1), using the boundary model in two different ways.

3.1. *Global Boundary Estimator Based on Complete Cubic Splines*

Let $g(y)$ denote the function to be approximated by a complete cubic spline on the interval $\alpha \le y \le \beta$. For the sequence of equidistant knots $y_{i+1} = \alpha + ih$, $i = 0, 1, \ldots, n$ and $h = (\beta - \alpha)/n$, denote the values of function g and its first derivative with respect to y at the jth knot by g_j and g_j', respectively. Then, the cubic polynomial

$$\bar{f}_i(\eta) = \sum_{j=1}^{n+1} a_{ij}(\eta)g_j + b_{i1}(\eta)g_1' + b_{i(n+1)}(\eta)g_{n+1}', \quad i = 1, 2, \ldots, n \tag{3}$$

approximates g in the ith interval (for details see [4, 11]). In Eq. (3), η is a local coordinate for the ith interval (Fig. 2) defined as $\eta = y - y_i$ $(0 \le \eta \le h)$,

$$a_{ij}(\eta) = \frac{(h-\eta)^3 - h^2(h-\eta)}{6h}\omega_{ij} - \frac{\eta(h^2-\eta^2)}{6h}\omega_{(i+1)j} + \delta_{ij}\frac{h-\eta}{h} + \delta_{(i+1)j}\frac{\eta}{h},$$

$$b_{i1}(\eta) = \frac{(h-\eta)^3 - h^2(h-\eta)}{6h}\sigma_{i1} - \frac{\eta(h^2-\eta^2)}{6h}\sigma_{(i+1)1},$$

and

$$b_{i(n+1)}(\eta) = \frac{(h-\eta)^3 - h^2(h-\eta)}{6h}\sigma_{i(n+1)} - \frac{\eta(h^2-\eta^2)}{6h}\sigma_{(i+1)(n+1)},$$

where $[\omega_{ij}] = [C]^{-1}[D]$, $[\sigma_{ij}] = [C]^{-1}$,

$$C = \begin{bmatrix} 1/3 & 1/6 & 0 & 0 & \cdots & 0 & 0 \\ 1/6 & 2/3 & 1/6 & 0 & \cdots & 0 & 0 \\ 0 & 1/6 & 2/3 & 1/6 & \cdots & 0 & 0 \\ \cdot & \cdot & \cdot & \cdot & \cdots & \cdot & \cdot \\ 0 & 0 & 0 & 0 & \cdots & 1/6 & 1/3 \end{bmatrix} h,$$

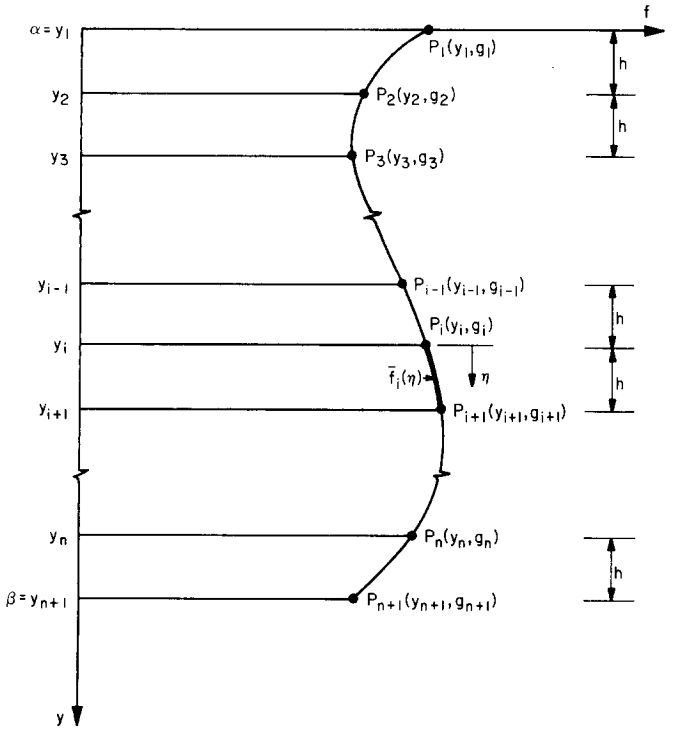

FIG. 2. Complete cubic spline function $f(y)$ interpolating $g(y)$ at points $P_i(y_i, g_i)$, $i = 1, 2, \ldots, n + 1$. Equidistant knots.

$$D = \begin{bmatrix} -1 & 1 & 0 & 0 & \cdots & 0 & 0 \\ 1 & -2 & 1 & 0 & \cdots & 0 & 0 \\ 0 & 1 & -2 & 1 & \cdots & 0 & 0 \\ \cdot & \cdot & \cdot & \cdot & \cdots & \cdot & \cdot \\ 0 & 0 & 0 & 0 & \cdots & 1 & -1 \end{bmatrix} 1/h,$$

and δ_{ij} is the Kronecker delta. Both C and D are nonsingular, symmetric, tridiagonal, $(n + 1) \times (n + 1)$ matrices. It is noted that the cubic polynomial $\bar{f}_i(\eta)$ depends linearly on all function values g_i and the slopes g'_1 and g'_{n+1} at the extreme knots. The resulting complete cubic splines, $f(y)$, approximating the function $g(y)$ on $[\alpha, \beta]$ is given by

$$f(y) = \sum_{i=1}^{n} \delta_i \bar{f}_i(\eta), \tag{3a}$$

where $\delta_i = 1$ if $y_i < y < y_{i+1}$, and $\delta_i = 0$ otherwise.

The state vector in this formulation is chosen to be $\mathbf{x}^T = [g_1, g_2, \ldots, g_{n+1}, g'_1, g'_{n+1}]$. Consequently, the system matrix Φ_k [Eq. (1)] becomes the $(n + 3) \times (n + 3)$ identify matrix. At $y = \bar{y}_i = \text{const}$ the quantity $(p_i - p_b)$ is measured. For enhanced observability, n simultaneous measurements are performed. At the kth cycle of the filtering process, measurements of $(p_i - p_b)$ are performed at $\bar{y}_i^k = \alpha + k + (i - 1)h$, $i = 1, 2, \ldots, n$, and arranged into a column vector $z_k = [z_1^k, z_2^k, \ldots, z_n^k]^T$. Based on Eqs. (2) and (3), $(p_i - p_b)$ can be easily expressed as a linear combination of the states and consequently, the measurement matrix H_k takes the form

$$H_k = \frac{p_a - p_b}{l_w} \begin{bmatrix} a_{11} & a_{12} & \cdots & a_{1(n+1)} & b_{11} & b_{1(n+1)} \\ a_{21} & a_{22} & \cdots & a_{2(n+1)} & b_{21} & b_{2(n+1)} \\ \cdot & \cdot & \cdots & \cdot & \cdot & \cdot \\ a_{n1} & a_{n2} & \cdots & a_{n(n+1)} & b_{n1} & b_{n(n+1)} \end{bmatrix}.$$

For large values of k, the filter [Eq. (1)] converges to the true state vector. This allows the *global analytical* description of the boundary curve using Eqs. (3) and (3a).

3.2. *Boundary Point Estimator*

The objective of the boundary point estimator is to estimate positions of *individual* boundary points based on measurements performed in the ambiguity zone. In constructing the mathematical model for the boundary point estimator the imposition of interpolation conditions is abandoned. Furthermore, in order to be able to satisfactorily approximate boundaries with isolated discontinuities in their low-order derivatives, we have focused on spline approximations exhibiting good localization properties [4, 11]. Here, we present the development of system and measurement models for a cubic spline ($\kappa = 3$) with equidistant knots. The range of variable y is the interval $[\alpha, \beta]$. We assume equidistant knots $t_i = t_0 + ih$, $i = 0, 1, \ldots, n$, such that $\alpha = t_0$ and $t_n = \beta$ (Fig. 3). Introducing six extra knots outside the interval $[\alpha, \beta]$, three at each end, we obtain the augmented sequence of knots $t_i = t_0 + ih$, $i = -3, -2, \ldots, n + 3$. On this knot sequence, we define $(n + 3)$ B-splines of degree κ using

$$B_p^\kappa(y) = \sum_{j=p}^{p+\kappa+1} \left[\prod_{\substack{i=p \\ i \neq j}}^{p+\kappa+1} \frac{1}{(t_i - t_j)} \right] (y - t_j)_+^\kappa, \tag{4}$$

$$p = -\kappa, -\kappa + 1, \ldots, n - 1,$$

where

$$(y - t_j)_+^\kappa = \begin{cases} (y - t_j)^\kappa & \text{if } y \geq t_j \\ 0 & \text{if } y < t_j. \end{cases}$$

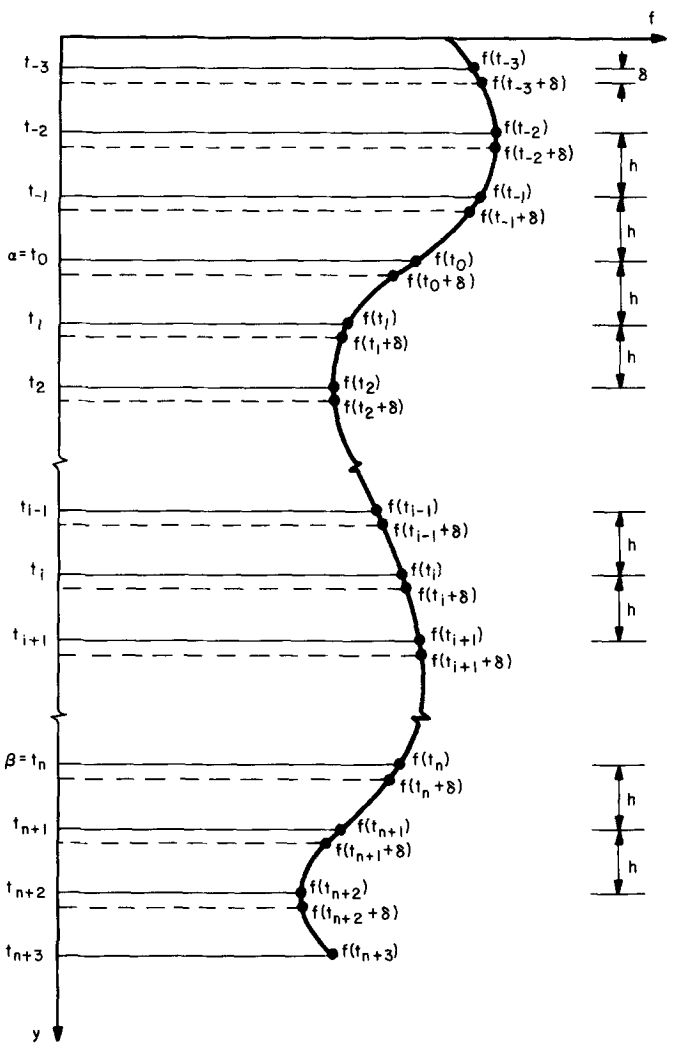

FIG. 3. Knot arrangement for the boundary point estimator.

For the special case of equidistant knots and $\kappa = 3$ we have

$$B_p^3(y) = \frac{1}{24h^4}[(y - t_p)_+^3 - 4(y - t_{p+1})_+^3 + 6(y - t_{p+2})_+^3 - 4(y - t_{p+3})_+^3 + (y - t_{p+4})_+^3], \quad (5)$$
$$p = -3, -2, \ldots, n - 1.$$

By forming the vectors

$$\tilde{\mathbf{f}} = [f(t_0), f(t_1), \ldots, f(t_{n-1})]^T, \quad (6)$$
$$\mathbf{g} = [g(t_{-2}), g(t_{-1}), \ldots, g(t_{n+2})]^T, \quad (7)$$

and evaluating Eq. (5) at $y = t_p$, $p = 0, 1, \ldots, n - 1$, we obtain

$$\tilde{\mathbf{f}} = \tilde{E}\mathbf{g}, \quad (8)$$

where $\tilde{E}$ is an $n \times (n + 5)$ constant matrix defined by

$$\tilde{E} = \begin{bmatrix} a_1 & a_2 & a_3 & a_4 & a_5 & 0 & 0 & 0 & \cdot & \cdot & \cdot & 0 \\ 0 & a_1 & a_2 & a_3 & a_4 & a_5 & 0 & 0 & \cdot & \cdot & \cdot & 0 \\ \cdot & \cdot & \cdot & \cdot & \cdot & \cdot & \cdot & \cdot & \cdot & \cdot & \cdot & \cdot \\ 0 & 0 & \cdot & \cdot & \cdot & 0 & a_1 & a_2 & a_3 & a_4 & a_5 & 0 \end{bmatrix} \quad (9)$$

and $a_1 = -\frac{1}{36}$, $a_2 = \frac{1}{9}$, $a_3 = \frac{5}{6}$, $a_4 = \frac{1}{9}$, $a_5 = -\frac{1}{36}$. By expanding vector $\tilde{\mathbf{f}}$ to

$$\mathbf{f} = [f(t_{-2}), f(t_{-1}), f(t_0), f(t_1), \ldots, f(t_n), f(t_{n+1}), f(t_{n+2})]^T \quad (10)$$

and introducing the square matrix, E, defined by

$$E = \begin{bmatrix} 1 & & & & & & \\ & 1 & & & & & \\ & & \tilde{E} & & & & \\ & & & 1 & & & \\ & & & & 1 & & \\ & & & & & 1 \end{bmatrix}, \quad (11)$$

Eq. (8) is rewritten as

$$\mathbf{f} = E\mathbf{g}. \quad (12)$$

Considering a set of points displaced by δ pixels (relative to t_i, $i = -2, -1, \ldots, n + 2$, see also Fig. 3) in the y-direction we can similarly write

$$\mathbf{f}_\delta = F\mathbf{g}, \quad (13)$$

where F is an $(n + 5) \times (n + 5)$ matrix given by

$$F = \begin{bmatrix} 1 & 0 & 0 & \cdot & \cdot & \cdot & \cdot & \cdot & \cdot & \cdot & \cdot & \cdot & \cdot & 0 \\ 0 & 1 & 0 & \cdot & \cdot & \cdot & \cdot & \cdot & \cdot & \cdot & \cdot & \cdot & \cdot & 0 \\ b_1 & b_2 & b_3 & b_4 & b_5 & b_6 & 0 & 0 & \cdot & \cdot & \cdot & \cdot & \cdot & 0 \\ 0 & b_1 & b_2 & b_3 & b_4 & b_5 & b_6 & 0 & \cdot & \cdot & \cdot & \cdot & \cdot & 0 \\ \cdot & \cdot & \cdot & \cdot & \cdot & \cdot & \cdot & \cdot & \cdot & \cdot & \cdot & \cdot & \cdot & \cdot \\ 0 & 0 & \cdot & \cdot & \cdot & \cdot & \cdot & 0 & b_1 & b_2 & b_3 & b_4 & b_5 & b_6 \\ 0 & 0 & \cdot & \cdot & \cdot & \cdot & \cdot & 0 & 0 & 0 & 0 & 1 & 0 & 0 \\ 0 & 0 & \cdot & \cdot & \cdot & \cdot & \cdot & \cdot & \cdot & \cdot & \cdot & 0 & 1 & 0 \\ 0 & 0 & \cdot & \cdot & \cdot & \cdot & \cdot & \cdot & \cdot & \cdot & \cdot & 0 & 0 & 1 \end{bmatrix} \quad (14)$$

and $\mathbf{f}_\delta = [f(t_{-2} + \delta), f(t_{-1} + \delta), \ldots, f(t_{n+1} + \delta), f(t_{n+2} + \delta)]^T$. The elements of matrix F are

$$b_1 = \frac{1}{36h^3}[-(3h + \delta)^3 + 4(2h + \delta)^3 - 6(h + \delta)^3 + 4\delta^3], \quad (15)$$

$$b_2 = \frac{1}{36h^3}[8(3h + \delta)^3 - 33(2h + \delta)^3 + 52(h + \delta)^3 - 38\delta^3], \quad (16)$$

$$b_3 = \frac{1}{36h^3}[-(3h + \delta)^3 + 12(2h + \delta)^3 - 39(h + \delta)^3 + 56\delta^3], \quad (17)$$

$$b_4 = \frac{1}{36h^3}[-(2h + \delta)^3 + 12(h + \delta)^3 - 39\delta^3], \quad (18)$$

$$b_5 = \frac{1}{36h^3}[-(h + \delta)^3 + 12\delta^3],$$

and

$$b_6 = -\frac{1}{36h^3}\delta^3. \quad (20)$$

Combining Eqs. (12) and (13) we obtain

$$\mathbf{f}_\delta = \Phi\mathbf{f}, \quad (21)$$

where

$$\Phi = FE^{-1}. \quad (22)$$

Equation (21) relates two sets of points on the boundary separated by distance δ in the y-direction.

The state vector, $\mathbf{x}$, in this formulation is chosen to be equal to vector $\mathbf{f}$ defined in Eq. (10); i.e., the state vector contains the values of the approximating spline function at the knots $t_j, j = -2, -1, \ldots, n + 2$. At each cycle of the filtering process, the knot sequence $t_j, j = -3, -2, \ldots, n + 3$, is displaced by δ pixels in the direction of increasing y. Then, in view of Eq. (21), Eq. (1) is satisfied at the kth step of the filtering process with $\mathbf{x}_k = \mathbf{f}$, $\mathbf{x}_{k+1} = \mathbf{f}_\delta$, and $\Phi_k = \Phi$.

For the boundary point estimator the measurable quantity used at $y = \bar{y}_i = \text{const}$ is

$$q(y = \bar{y}_i) = \frac{l_w(p_i - p_b)}{p_a - p_b}. \quad (23)$$

At the kth cycle of the filtering process, measurements of $q(y = t_j)$ are performed for $j = -2, -1, \ldots, n + 2$ and arranged into a column vector $z_k = [z^k_{-2}, z^k_{-1}, \ldots, z^k_{n+2}]$. Then, taking into account Eq. (2) and the definition of the state vector, H_k becomes the $(n + 5) \times (n + 5)$ identity matrix. It is noted that the data needed for measurements outside the interval $[\alpha, \beta]$ are generated by first reflecting the image about the lines parallel to the f-axis at locations $(t_0, f(t_0))$ and $(t_n, f(t_n))$ and then reflecting the result about the lines parallel to the y-axis at locations $(t_0, f(t_0))$ and $(t_n, f(t_n))$.

4. DISCUSSION AND RESULTS

The boundary detection methods using the proposed models have been successfully applied to a number of images. The performance of the global boundary estimator, which provides a means of obtaining an analytic description of smooth boundaries, is illustrated by the examples shown in Figs. 4, 6a, and 6c. The point estimator detects very accurately individual boundary points, as illustrated by the examples in Figs. 5, 6b, and 6d. The point estimator performs well on boundaries that have discontinuities in low order derivatives and corners. Examples of its performance in such cases are discussed in [8].

The correct choice of property p, Eqs. (2) and (23), is crucial for the success of the segmentation schemes described in Sections 2 and 3. It is necessary that the selected property allows differentiation between the regions involved. The results shown in this paper are obtained using region mean gray level. In this case, $p_a = \mu_a$, $p_b = \mu_b$, and $p_i = \mu_w$, where μ_a and μ_b denote region means for regions A and B, respectively, and μ_w is the mean of the window $s \times l$ centered (in the y-direction) at $y = y_i$ in W. In this paper we use $s = l_w$ and $l = 1$. When regions are not characterized by uniform intensity, the described formulations can be applied by using cooccurrence matrices [7]. Linear dependence on the states, required by the measurement model [Eq. (1)], is achieved by using linear combinations of the elements of the cooccurrence matrix as described in [3].

Sensitivity analysis of the boundary estimators reveals that

- The estimators are relatively insensitive to system modeling errors. This is attributed to the ability of spline functions to conform with the local behavior of the boundary curves. Furthermore, both estimators are found to be insensitive to errors in the initial state estimate $\mathbf{x}_0$.
- When determining smooth boundaries, the results are not significantly affected by the number of knots. Table 1 lists the mean square error as a function of number of knots for the boundary geometry shown in Figs. 4 and 5. The accuracy of the boundary approximation increases as the number of knots increases.
- The state estimates are sensitive to the measurement error covariance matrix R_k. When considering uniform regions with noise of known standard deviation, the diagonal elements of the R_k matrix can be calculated; otherwise, it is necessary to use a method for automatic noise

TABLE 1
Effects of Number of Knots on the Root Mean Square Error for the Geometry Shown in Figs. 4 and 5 (Noise—σ = 40)

n	Global boundary estimator	Boundary point estimator
4	0.132	0.276
6	8.99×10^{-2}	0.138
8	7.20×10^{-2}	7.05×10^{-2}
10	6.97×10^{-2}	4.80×10^{-2}
12	5.83×10^{-2}	4.23×10^{-2}

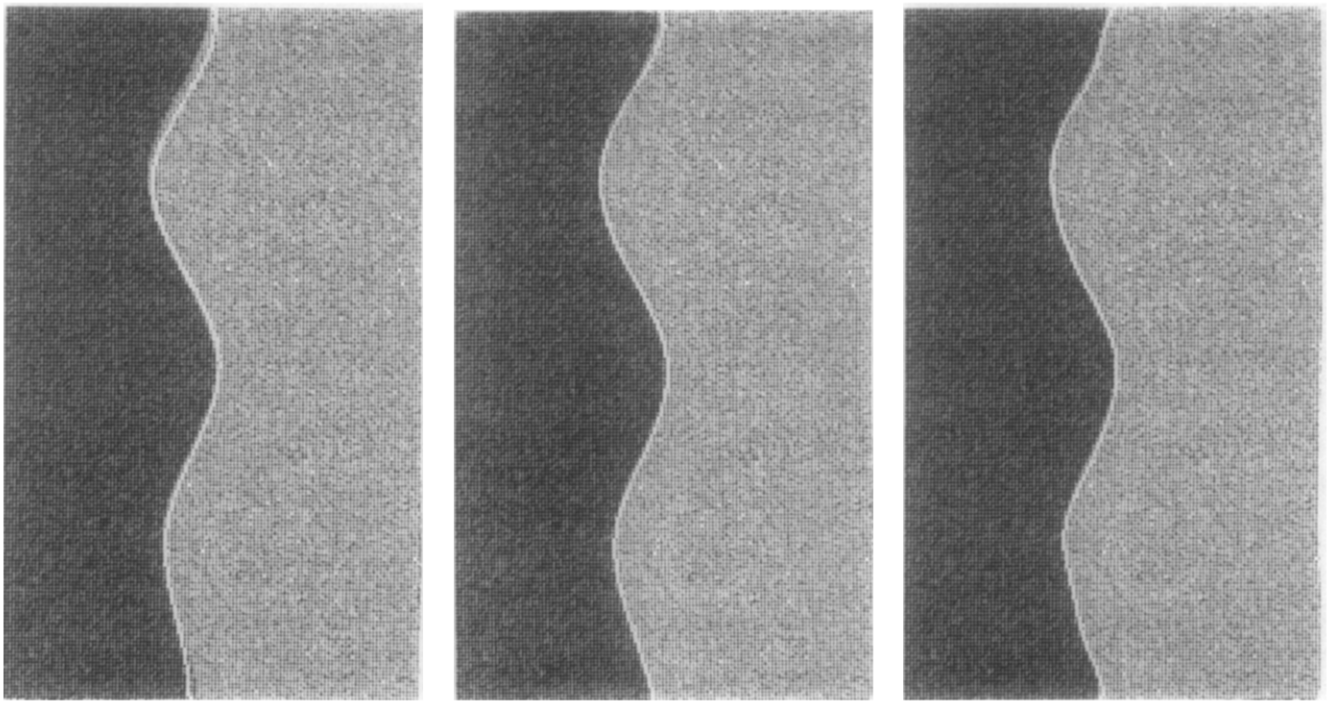

$n = 4,\ \sigma = 40$ $n = 8,\ \sigma = 40$ $n = 12,\ \sigma = 40$

a

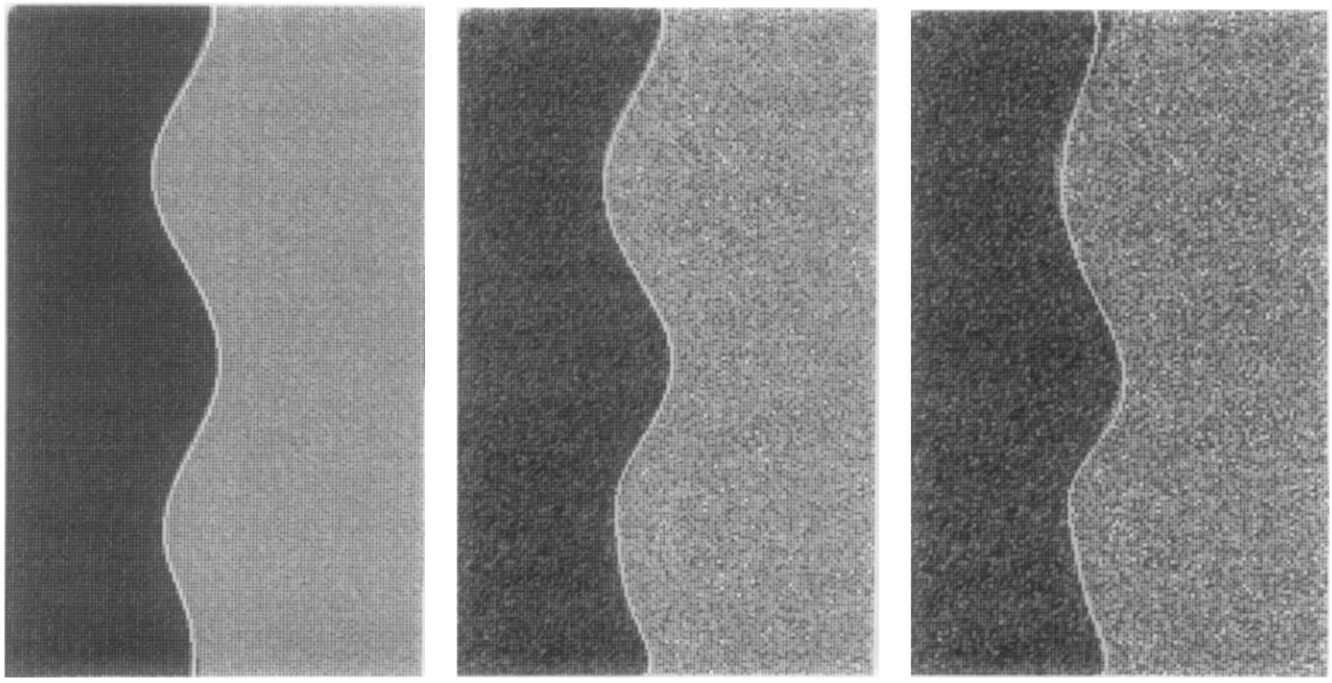

$n = 10,\ \sigma = 20$ $n = 10,\ \sigma = 60$ $n = 10,\ \sigma = 100$

b

FIG. 4. Global boundary estimator: (a) effects of number of knots, (b) effects of noise.

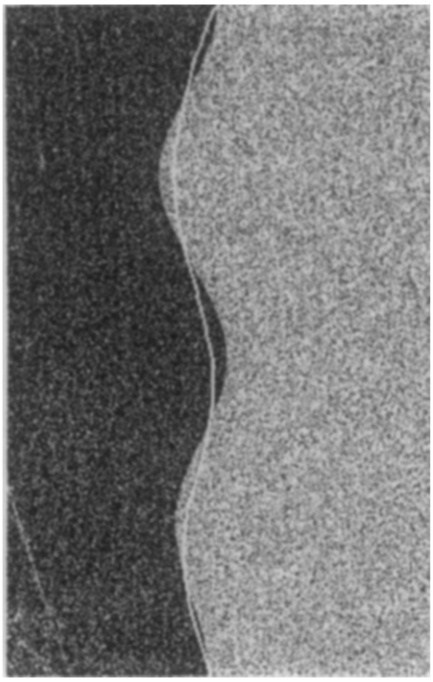

$n = 4,\ \sigma = 40$

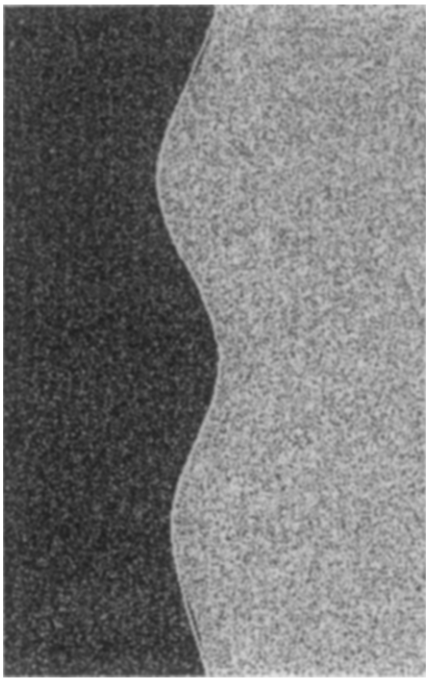

$n = 8,\ \sigma = 40$

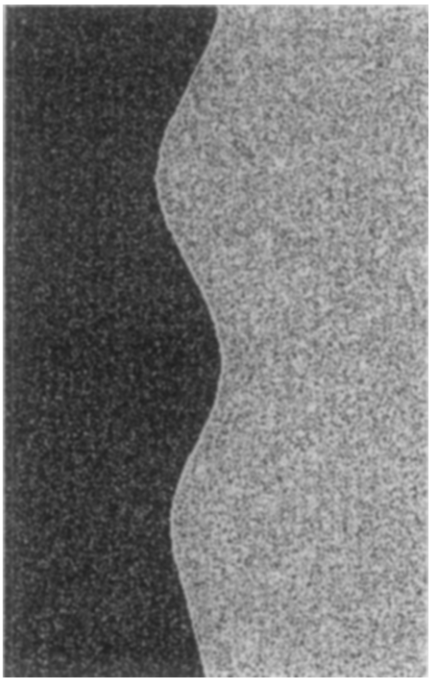

$n = 12,\ \sigma = 40$

a

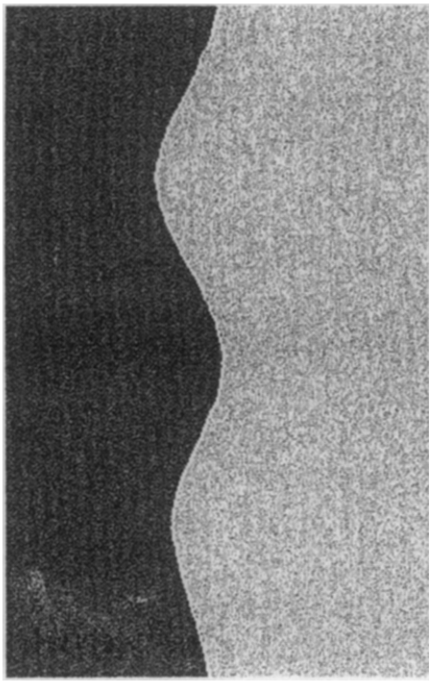

$n = 10,\ \sigma = 20$

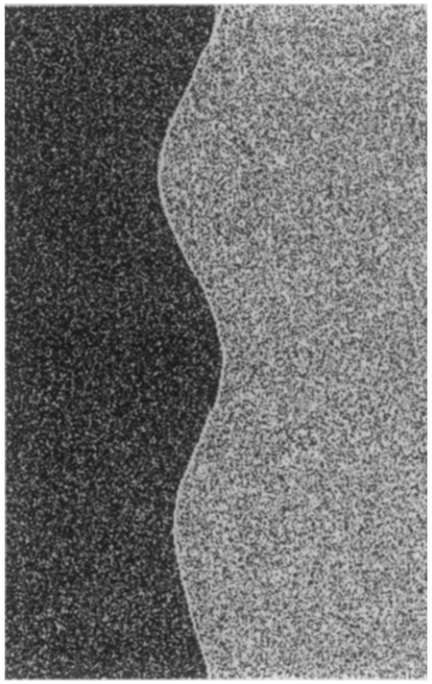

$n = 10,\ \sigma = 60$

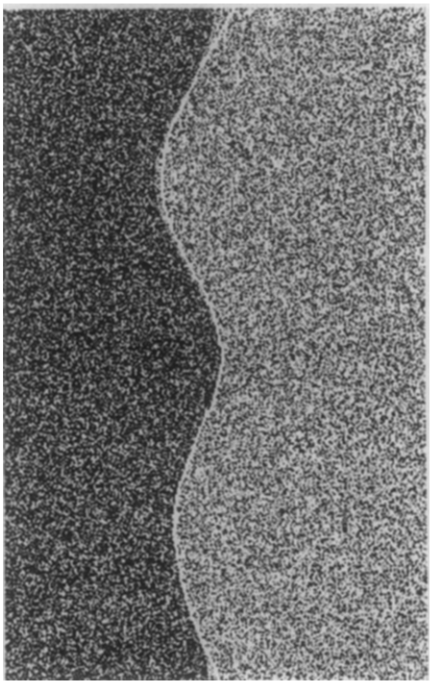

$n = 10,\ \sigma = 100$

b

FIG. 5. Boundary point estimator: (a) effects of number of knots, (b) effects of noise.

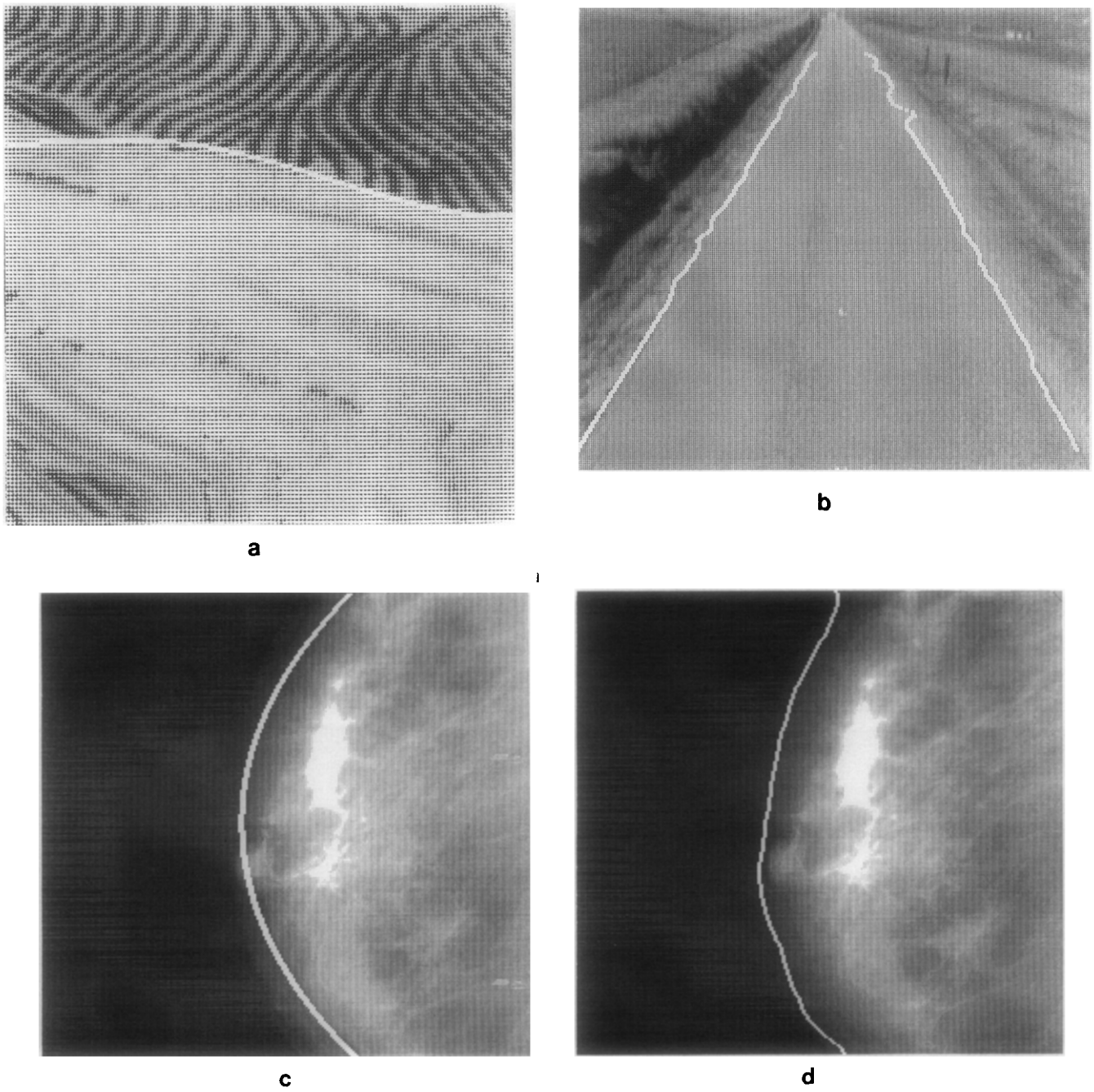

FIG. 6. Application to real images: (a) global estimator applied to texture image, (b) point estimator applied to road image, (c)–(d) separation of object from the background in mammogram analysis, global and point estimators, respectively.

estimation. In this work we have used the method described in [12].

The proposed boundary estimators are capable of performing very well in the presence of noise as illustrated by Table 2 and Figs. 4b and 5b. In general, the root mean square error increases as the noise increases; however, very good results are obtained even in cases with high levels of noise as can be seen from Table 2.

The proposed methods, besides detecting a boundary, also provide analytic boundary description, in contrast to

TABLE 2
Effects of Noise on the Root Mean Square Error for the Geometry Shown in Figs. 4 and 5 (Using $n = 10$)

σ	Global boundary estimator	Boundary point estimator
0	4.2×10^{-2}	1.78×10^{-7}
20	5.98×10^{-2}	3.33×10^{-2}
40	6.97×10^{-2}	4.80×10^{-2}
60	9.78×10^{-2}	7.05×10^{-2}
80	0.124	0.109
100	0.176	0.161

typical edge detection methods. Moreover, they detect low contrast edges between noisy regions or texture regions, when using an appropriate measurement model. Utilization of LRF makes the methods well suited for real time applications and cases where available memory is limited; in addition, LRF provides an insight into the uncertainty of the obtained boundary through the estimation of the error covariance matrix.

APPENDIX: LIST OF SYMBOLS

a_{ij}, b_{i1}, $b_{i(n+1)}$	Cubic polynomials in η (Section 3.1)
b_i, $i = 1, 2, \ldots, 6$	See Eqs. (15)–(20)
$\bar{f}_i(\eta)$	Cubic polynomial approximating g in the ith interval [Eq. (3)]
f	Spline function approximating function g
g	Function defining the boundary curve
g_j	$g(y_j)$
h	Distance between knots in equidistant knot arrangement
l_a, l_b	Widths of the homogeneous regions A and B at $y = y_i$
l_w	Width of the ambiguity zone at $y = y_i$
n	Number of segments in $[\alpha, \beta]$
p_a, p_b	Values of property p in regions A and B, respectively
p_i	Value of property p in the ambiguity zone, W, at $y = y_i$
q	Measurable quantity used by the boundary point estimator
$t_j, j = 0, 1, \ldots, n$	Knot sequence for boundary point estimator
$\mathbf{v}_k$	Measurement noise vector at step k
$\mathbf{w}_k$	System noise vector at step k
$\mathbf{x}_k$	State vector at step k
$y_j, j = 1, 2, \ldots, n+1$	Knot sequence for global estimator
$\bar{y}_j, j = 1, \ldots, n$	Locations of simultaneous measurements
$\bar{y}_i^k, i = 1, 2, \ldots, n$	Positions of simultaneous measurements for global estimator
$\mathbf{z}_k$	Measurement vector at step k
A, B	Homogeneous regions
B_j^κ	jth B-spline of degree κ
C, D	Matrices (Section 3.1)
$\tilde{E}$, E, F	Matrices (Section 3.2)
H_k	Measurement matrix at step k
$N(0, G)$	Normal distribution with zero mean and covariance matrix G
Q_k	System noise covariance matrix at step k
R_k	Measurement noise covariance matrix at step k
W	Ambiguity zone

Greek Symbols

δ	y component of displacement for boundary point estimator
δ_{ij}	Kroneckers delta
η	Local coordinate, $\eta = y - y_i$, $0 \le \eta \le h$
κ	Degree of spline function
μ_a, μ_b, μ_w	Region means for regions A, B, and W, respectively
ρ_i	Boundary coordinate, local in W, at $y = y_i$ (Fig. 1)
σ	Standard deviation of noise
Φ_k	System matrix at step k

REFERENCES

1. M. Basseville, B. Espiau, and J. Gasnier, Edge detection using sequential methods for change in level. I. A sequential edge detection algorithm, *IEEE Trans. Acoust. Speech Signal Process.* **ASSP 29,** No. 1, 1981, 24–31.
2. M. Basseville, Edge detection using sequential methods for change in level II. Sequential detection of change in mean, *IEEE Trans. Acoust. Speech Signal Process.* **ASSP 29,** No. 1, 1981, 32–50.
3. D. Brzakovic and A. Liakopoulos, Measurement models for sequential estimation of boundaries in digital images, in *Proceedings, IASTED International Symposium: Applied Signal Processing, Paris, France, 1985,* pp. 168–172.
4. C. De Boor, *A Practical Guide to Splines,* Springer-Verlag, New York, 1978.
5. A. Gelb, *Applied Optimal Estimation,* MIT Press, Cambridge, MA, 1974.
6. S. Grinaker, Edge based segmentation and texture separation, in *Proceedings, 5th International Conference on Pattern Recognition, Miami Beach, Florida, 1980,* pp. 554–557.
7. R. M. Haralick, Statistical and structural approaches to texture, *Proc. IEEE* **67,** No. 5, 1979, 786–803.
8. L. Hong, D. Brzakovic, and A. Liakopoulos, Boundary detection in digital images based on spline functions and estimation theory, in *Proceedings, 26th IEEE Conference on Decision and Control, Los Angeles, Ca, 1987,* pp. 1048–1049.
9. R. E. Kalman, New methods in Wiener filtering theory, in *Proc. of the 1st Symposium on Engineering Applications, Random Function Theory and Probability,* Wiley, New York, 1963.
10. M. Kass, A. Witkin, and D. Terzopoulos, Snakes: Active contour models, in *Proceedings, First International Conference on Computer Vision, London, England, 1987,* pp. 259–268.
11. M. J. D. Powell, *Approximation Theory and Methods,* Cambridge Univ. Press, Cambridge, MA, 1981.
12. H. Sari-Sarraf and D. Brzakovic, Automated iterative noise filtering, *IEEE Trans. on Acoustics, Speech and Signal Processing.* **ASSP39,** No. 1, 1991, 23–242.